International Journal of Biological Macromolecules 140 (2019) 415–422

Contents lists available at ScienceDirect

International Journal of Biological Macromolecules

journal homepage: http://www.elsevier.com/locate/ijbiomac

Voltammetric measurements of neurotransmitter-acetylcholine through metallic nanoparticles embedded 2-D material

Chetna Tyagi [a], Nidhi Chauhan [b], Ambuj Tripathi [a], Utkarsh Jain [b,*], D.K. Avasthi [b,*]

[a] Inter-University Accelerator Centre, Aruna Asaf Ali Marg, New Delhi 110067, India
[b] Amity Institute of Nanotechnology, Amity University, Noida 201303, Uttar Pradesh, India

ARTICLE INFO

Article history:
Received 20 May 2019
Received in revised form 6 August 2019
Accepted 12 August 2019
Available online 14 August 2019

Keywords:
Acetylcholine
Gold- graphene oxide nanocomposite
Biosensor
Acetylcholinesterase

ABSTRACT

The most generally spread neurotransmitter acetylcholine (Ach) is used as a chemical messenger assisting in conveying signals transversely through the nerve synapse. Herein, two enzymes acetylcholinesterase and choline oxidase were covalently immobilized over the gold nanoparticles (Au_{NPs}) embedded graphene oxide (GO; 2D carbon material) nanocomposite modified ITO coated glass plate. The synergetic and unique properties of Au_{NPs} and GO present in nanocomposite are used to detect the ultra-small concentration of analyte, Ach. The prepared nanocomposites were characterized using different techniques i.e. TEM, XRD, SEM, FTIR, UV–Vis and Raman Spectroscopy. All the electrochemical measurements were performed using 3 electrodes integrated electrochemical system by introducing Ach through varying its concentration from 100 pM to 1000 nM. Cyclic voltammetry curves for different concentrations of Ach indicate the facile charge transfer process over the working electrode. Square wave voltammetry curves indicate the good sensing measurements of the modified electrode at the fixed potential. The limit of detection was found to be as low as 100 pM. In addition to these, selectivity of the electrode towards Ach molecule was confirmed by measuring the response towards other interfering agents. Besides this, the present nano interface is capable of detecting Ach in biological fluid such as serum.

1. Introduction

Choline is a nutrient which is vital for human brain development specifically crucial for cellular growth. Hence, its intake in daily diet in organisms is required for proper functioning of brain and healthy life [1]. Few animals cannot synthesize choline, but must consume it in their diet to stay healthy. Humans can produce choline in the liver in small quantity. Also, choline takes part in the production of acetylcholine (Ach) which is an important neurotransmitter in both nervous systems: central and peripheral. The quantity of Ach produced in body should not be below certain level as the decrement in its level leads to several nervous disorders like Alzheimer's disease, Parkinson's disease, Huntington disease and multiple sclerosis [2]. So, the detection of Ach is important for diagnosis of nervous system related disorders. Various methods of detection for Ach are available such as, high-pressure liquid chromatography (HPLC) [3], gas chromatography with mass spectrometry (GC–MS) [4], radioimmunoassay [5], colorimetric methods [6] and chemiluminescence [7]. Novel electrochemical methods of Ach detection had also been reported. These methods were characterized with excellent sensitivity and specificity. An Ach sensor comprised of co-immobilized enzymes choline oxidase (ChO) and acetylcholinesterase (AchE) on the exterior of iron oxide nanoparticles (Fe_3O_4 NPs) with poly(3,4-ethylenedioxythiophene) polymer and rGO decorated fluorine doped tin oxide (FTO) [8]. A bienzymatic metal organic framework (MOF) amended gold electrode was also constructed to detect Ach in aqueous samples [9]. Another such biosensor utilizes the bienzymatic system coated on the surface of platinum nanoparticles and graphene modified ITO electrode [10]. Different other graphene/graphene oxide nanocomposites based biosensors are also reported in literature for the detection of Ach [11,12]. These methods provide rapid detection with enhanced specificity and sensitivity with long shelf life. However, it is known that detection of Ach is challenging due to the absence of any electro-active or chromophore group.

Previous reports have shown that carbon-based nano materials are non-toxic as well as biocompatible suitable for their utilization as biosensors [13–16]. Like, carbon nanotubes (CNTs) [17] along with metal nanoparticles [18] have shown their potential application in electrochemical biosensing. Also, graphene which contains only sp^2 bonded carbon atoms is being used for sensing applications. However, graphene has advantage over CNTs in electrochemistry due to its high specific surface area [19]. Graphene oxide (GO), an oxidized form of graphene have oxygen-moieties like epoxy, carboxyl and hydroxyl [20]. Its synthesis is very simple as compared to graphene and it can be reduced to obtain graphene-like properties [21]. Due to the presence of functional groups on edges and basal planes of GO, it is being used as an efficient matrix for

* Corresponding authors.
E-mail addresses: ujain@amity.edu (U. Jain), dka4444@gmail.com (D.K. Avasthi).

https://doi.org/10.1016/j.ijbiomac.2019.08.102
0141-8130/

preparing nanocomposites [22]. Literature shows that various nanocomposites prepared by decorating metal nanoparticles (like Au [23], Ag [24], Pt [25] and Pd [26]) on GO were used for enhancing sensing ability of biosensors. In addition, gold being biocompatible, is considered outstanding in form of nanostructures with different shape as metal and widely used in biomedical applications [27]. Specifically, the importance of combining Au_{NPs} with GO lies in providing better analytical properties which have been used for biosensing the macromolecules e.g. cholesterol [28].

In the present study, we prepared gold nanoparticles-graphene oxide (Au_{NPs}-GO) nanocomposites to utilize the unique properties of Au_{NPs} and GO. Au_{NPs}, apart from being biocompatible and conductive, provide large surface area for detection of analyte. Glucose used as capping agent for Au_{NPs} also reduced graphene oxide partially in its vicinity increasing the conductivity. The nanocomposites were characterized using UV–Vis spectroscopy, Fourier transform infrared (FTIR) spectroscopy, X-ray diffraction (XRD) and Raman spectroscopy. The ITO electrode was modified with this nanocomposite and used for the co-immobilization of AchE-ChO. Electrochemical measurements were performed to study the sensing ability of AchE-ChO based Au_{NPs}-GO/ITO electrode towards Ach measurement.

2. Experimental section

2.1. Chemical and reagents

GO solutions purchased from Graphene Supermarket, USA. Chloroauric acid, glucose, monosodium and disodium phosphate salts, ferri–ferrocyanide, acetylcholinesterase and choline oxidase were brought from Sigma Aldrich. Acetylcholine iodide was brought from Sisco Research Laboratories Pvt. Ltd. Potassium ferricyanide, potassium ferrocyanide, NaCl, KCl, Na_2HPO_4 and KH_2PO_4 were acquired from Fisher Scientific. Ethanol and de-ionized water were utilized as solvents.

2.2. Characterization tools

X-ray diffraction pattern of AchE-ChO@Au_{NPs}-GO nanocomposite was obtained using D8 Bruker X-ray Diffractometer with Copper as source having the wavelength of 1.54 Å. Electronic transitions in nanocomposite were identified using Hitachi U-3300 double beam UV–visible spectrophotometer in the range of 200–800 nm wavelength. Verter 70 V, Bruker Optik High-resolution Fourier transform infra-red (HR-FTIR) spectroscopy was employed to identify different functional groups present in Au_{NPs}-GO nanocomposite. Raman spectroscopy of the nanocomposite was performed using Renishaw Invia Raman microscope using Argon laser of wavelength 514.5 nm. Micrographs were obtained to study the morphology of the sample using MIRA II LMH (TESCAN) field emission scanning electron microscope (FE-SEM) and detailed structure using transmission electron microscope (JEOL JEM-2100F). Bio-logic SAS (SP-200) three-electrode electrochemical system was used for electrochemical measurements. Ag/AgCl was used as the reference electrode, platinum wire as auxiliary electrode and AchE-ChO/Au_{NPs}-GO/ITO@ glass electrode was used as working electrode.

2.3. Preparation of AuNPs-GO nanocomposite

Commercially procured GO solution from USA Graphene Supermarket was used. Standard procedure was adopted for synthesizing glucose-capped Au_{NPs} in which glucose act as reducing agent for chloroauric acid and capping agent for Au_{NPs}. These nanoparticles were placed in the refrigerator to avoid any agglomeration. Then GO solution and Au_{NPs} were mixed in 0.5:1 ratio by continuous stirring for 1 h at ambient temperature. The resulting mixture was drop casted over the ITO@ glass plate electrode and dried at room temperature for 24 h. After drying, Au_{NPs}-GO/ITO@ glass was functionalized with chitosan. AchE and ChO solution were mixed in the ratio of 1:20. The Au_{NPs}-GO/ITO@ glass electrode was immersed in the enzyme solution for 24 h. The

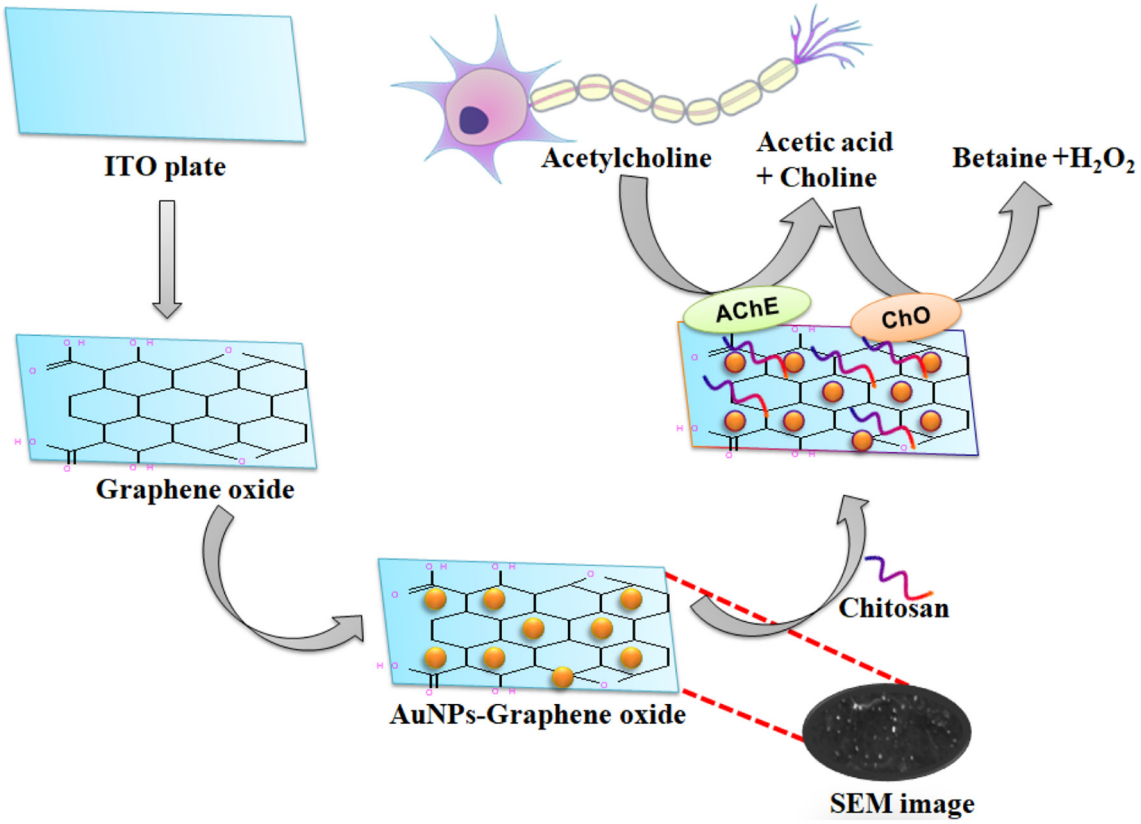

Fig. 1. Graphical representation for the stepwise preparation of working electrode and its mechanism to detect Ach.

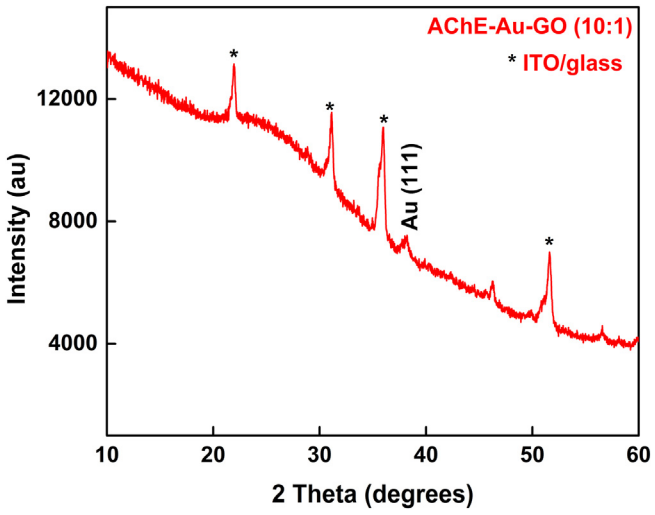

Fig. 2. XRD pattern of AchE-ChO/Au_{NPs}/GO (10:1) modified ITO@ glass electrode showing the peaks of Au_{NPs} and ITO substrate.

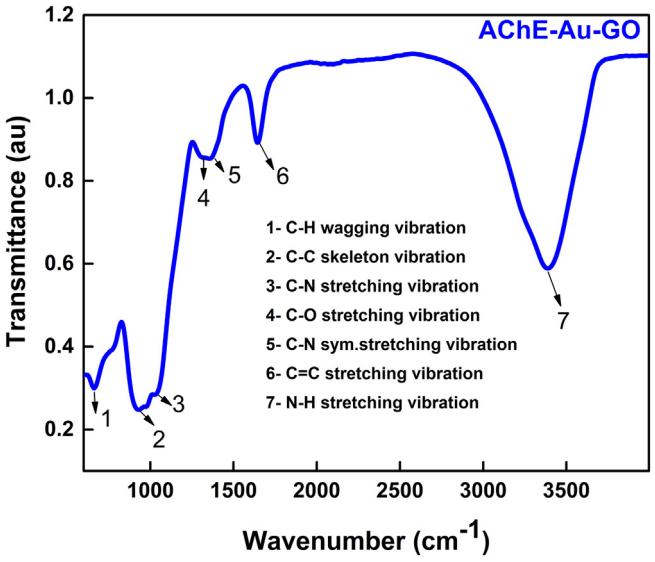

Fig. 4. FTIR spectrum of AchE-ChO/Au_{NPs}/GO nanocomposite indicating different functional groups present.

unbound enzyme on the surface of the AchE-ChO/Au_{NPs}-GO/ITO@ glass electrode was removed by using washing buffer to the surface of the electrode. The AchE-ChO/Au_{NPs}-GO/ITO@ glass electrode was constantly stored dry in a fridge at 4 °C. Electrochemical measurements were carried out to choose the electrode with better oxidation/reduction properties for further studies. Fig. 1 illustrates the stepwise modification of the working electrode we have used in the present work and enzymatic reactions involved in the detection mechanism of Ach in presence of AchE and ChO co-immobilized over the Au_{NPs}-GO/ITO@ glass electrode.

2.4. Electrochemical assay for the detection of Ach

The estimation of Ach and Ch depends upon the subsequent enzymatic reaction:

$$\text{Acetylcholine} + H_2O \xrightarrow{\text{AchE}} \text{Choline} + \text{Acetate}$$

$$\text{Choline} + O_2 \xrightarrow{\text{ChO}} \text{Betaine aldehyde} + H_2O_2$$

At the time of electrochemical sensing, enzymatic reaction leads to the formation of choline after interacting with substrate i.e. Ach in the presence of the enzyme AchE. The oxidation of H_2O_2 and thereby produced electrons (current) are linearly related to choline and in turn proportional to Ach concentration involved in the reaction.

CV measurements were performed using 3 electrode cell having 20 mL ferri/ferro solution as electrolyte (2.5 mM), 5 mL of 0.1 M sodium phosphate buffer (pH 7.5) and 0.1 mL of Ach (0.1 mM). The current (μA) was recorded through CV considering potential range in between −0.6 and + 0.6 V (vs Ag/AgCl). In order to evaluate the sensing performance, detection limit, response time and various concentrations of Ach on co-immobilized AchE-ChO over Au_{NPs}-GO/ITO@ glass electrode were studied.

2.5. Detection of Ach level in real samples

Five serum samples were procured from healthy individuals from Biodiagnostics Lab, Rohini, Sector-8, N. Delhi. In this analysis, cyclic voltammetry curves of the samples were obtained in which Ach was pre-

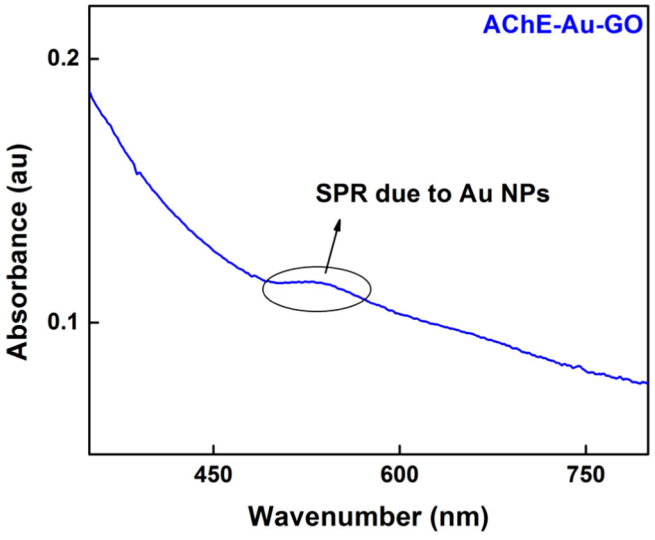

Fig. 3. UV–Visible absorption spectrum of Au_{NPs}/GO showing surface plasmon resonance (SPR) peak of Au_{NPs}.

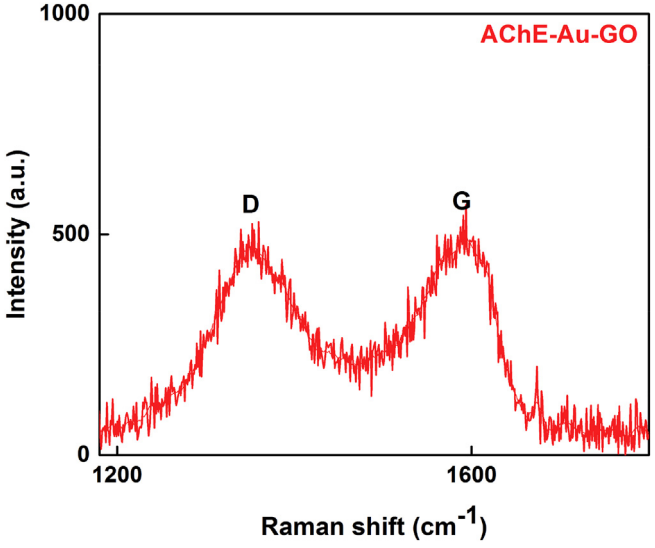

Fig. 5. Raman spectrum of AchE-ChO/Au_{NPs}/GO nanocomposite electrode showing D and G peaks as characteristics peaks of GO.

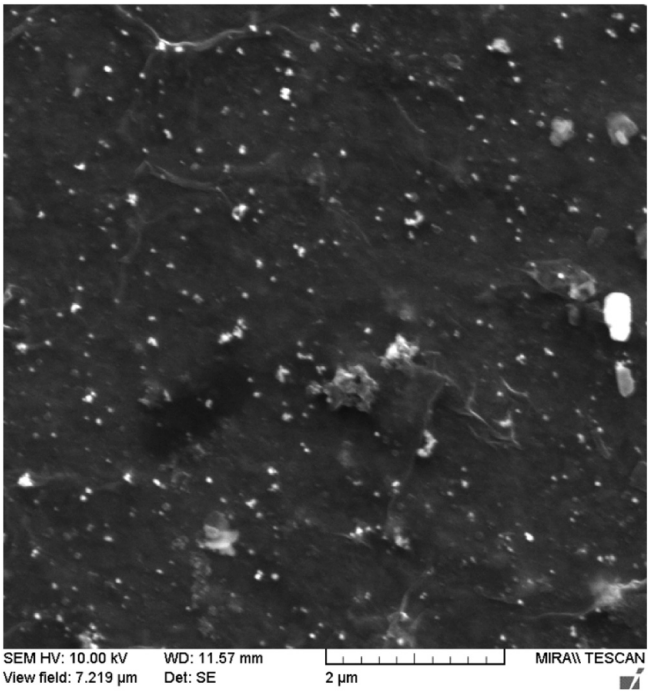

Fig. 6. Morphology of AchE-ChO/Au_{NPs}/GO film as seen in FE-SEM micrograph.

determined by the laboratory to compare the results of the present biosensor with the current technique employed in laboratory for Ach detection. The serum analysis was similar to reaction estimation excluding the analyte (Ach) which was replaced by serum sample.

3. Results and discussion

3.1. Characterizations

X-ray diffraction pattern of Au_{NPs}-GO electrode was obtained by applying the scan ranges from 10^0 to 60^0 (2θ) in locked coupled mode as shown in Fig. 2. The peaks at ~21.9^0, ~31.1^0, ~36.0^0 and 51.6^0 correspond to (211), (222), (400) and (440) planes of ITO electrode [29,30]. The peak at ~ 38.2^0 is due to (111) plane of Au_{NPs} present in Au_{NPs}-GO nanocomposite [31]. Fig. 3 shows UV–Visible spectrum (in absorbance mode) of the Au_{NPs}-GO/ITO@ glass electrode in the scan range of 350 nm to 800 nm with scan speed of 120 nm/min. A broad hump around 550 nm is observed due to the surface plasmon resonance of Au_{NPs} [27] indicating the presence of Au_{NPs}.

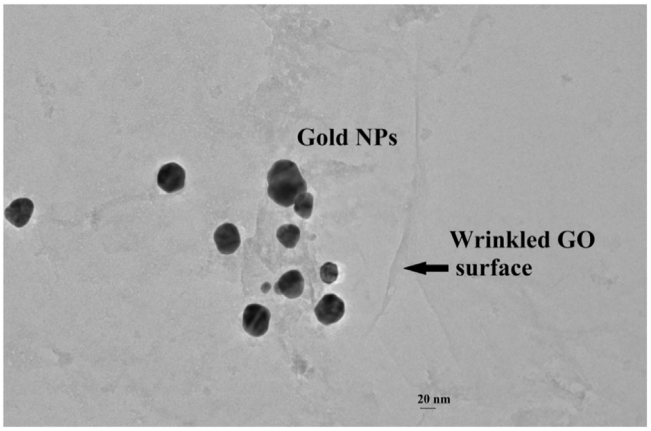

Fig. 7. TEM micrograph of Au_{NPs}/GO nanocomposite showing Au_{NPs} and GO surface.

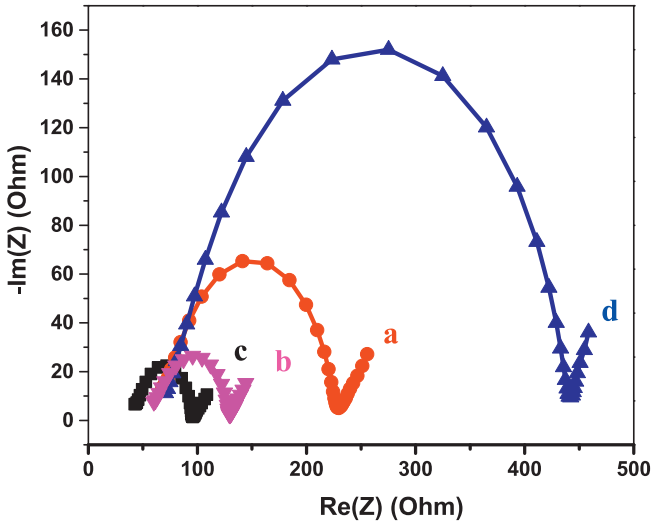

Fig. 8. EIS plot for bare ITO@ glass electrode (a), GO modified ITO@ glass electrode (b), Au_{NPs}/GO modified ITO@ glass electrode (c) and AchE-ChO/Au_{NPs}/GO modified ITO@ glass electrode (d) in ferri/ferro solution as electrolyte (2.5 mM) and sodium phosphate buffer (0.1 M, pH 7.5).

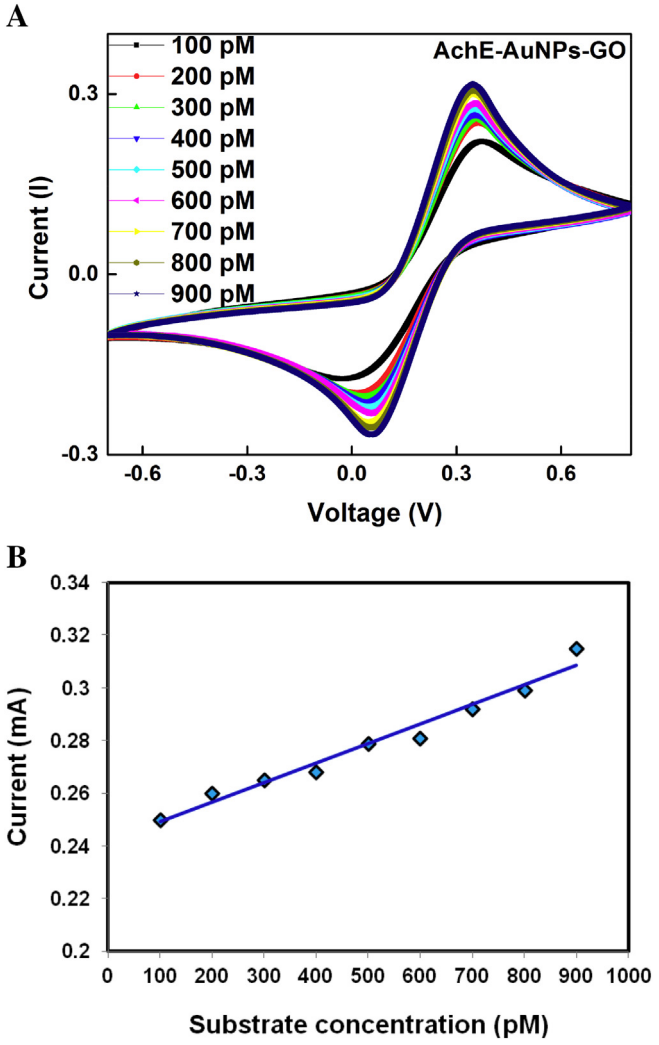

Fig. 9. A cyclic voltammetry plots for AchE-ChO/AuNPs/GO electrode in ferri/ferro solution as electrolyte (2.5 mM) and sodium phosphate buffer (0.1 M, pH 7.5) in the scan range of −0.7 to +0.8 V with varying concentration of Ach from 100 pM to 900 pM (for lower range). B. The calibration curve of Ach concentrations.

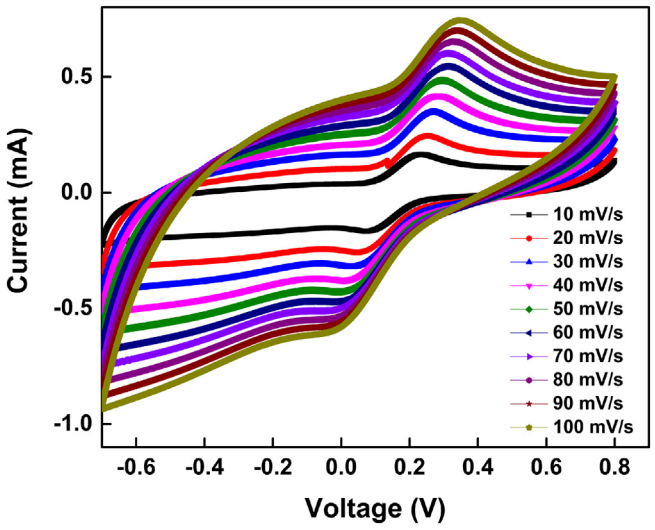

Fig. 10. Cyclic voltammetry curves for AchE-ChO/Au_{NPs}/GO modified ITO@ glass electrode in ferri/ferro solution as electrolyte (2.5 mM) and sodium phosphate buffer (0.1 M, pH 7.5) in the scan range of −0.7 to +0.8 V with different scan rates.

Different functional groups present in enzyme-coated Au_{NPs}-GO/ITO@ glass electrode were identified using Fourier transform infra-red spectroscopy in the scan range of 500–3999 cm^{-1} (Fig. 4). The bands at 1 and 2 correspond to C—H wagging and C—C skeleton vibrations, respectively [32]. As during the synthesis procedure, the enzymes, AchE and ChO were mixed and working electrode was immersed in it for bounding enzymes over it, signature of their bonding could be seen in FTIR spectrum. The bands 3, 5 and 7 are due to C—N and N—H stretching vibrations which indicate that AchE-ChO is attached to GO functional groups. C═C bonding of GO is indicated by the band at 6.

Raman spectroscopy is a vital tool for C-related materials as it is extremely susceptible to the graphitic and defective regions [33,34]. Raman spectroscopy was performed on the working electrode in the range of 1150–1800 cm^{-1} with the laser power of 5 mW for the exposure time of 20 s. The characteristics G and D peaks of GO at 1350 cm^{-1} and 1550 cm^{-1}, respectively, were identified as shown in Fig. 5. The G band corresponds to sp^2 hybridization of carbon rings and D band arises due to the O_2 including functional groups attached to edges and basal planes of GO.

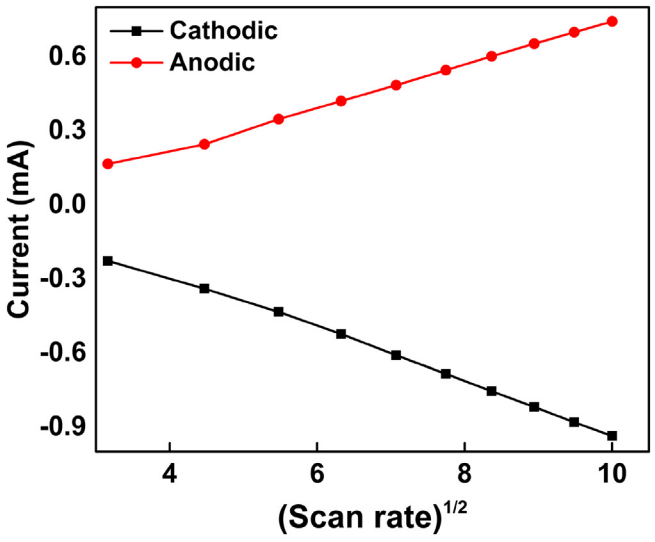

Fig. 11. Plot showing the linear behaviour of anode and cathode peak currents varying with the (scan rate)$^{1/2}$.

Surface morphology was studied using FE-SEM which shows the wrinkled surface of GO (Fig. 6). Transmission electron microscopy of Au_{NPs}-GO nanocomposite was performed using 200 keV electron beam as shown in the micrograph of Fig. 7. TEM micrograph is showing the wrinkled surface of GO sheets as well as the Au_{NPs} which are identified as the dark spherical structures adhered to the GO sheets.

The electrochemical impedance spectroscopy technique (EIS) was carried out to characterize the different stages for the preparation of working electrode. Fig. 8 represents the EIS curves of bare ITO@ glass electrode (a), GO/ITO@ glass electrode (b), Au_{NPs}-GO/ITO@ glass electrode (c) and AchE-ChO/Au_{NPs}-GO/ITO@ glass electrode (d), obtained in electrolytic solution of 0.1 M sodium phosphate buffer (pH 7.5) and 2.5 mM potassium ferricyanide and potassium ferrocyanide. It shows that bare ITO@ glass possesses the highest Ret (230 Ω) and it is decreased to 130 Ω while modified with GO. Subsequently, Au_{NPs}-GO/ITO@ glass electrode showed the most lowest Ret of 100 Ω, due to the high conductivity of the material. After immobilization of enzymes over the NPs modified electrode Ret increased upto 440 Ω (d), it showed greater hindrance to electron transfer. Since enzymes are biomolecules, resulting in causing obstruction for the transfer of electrons

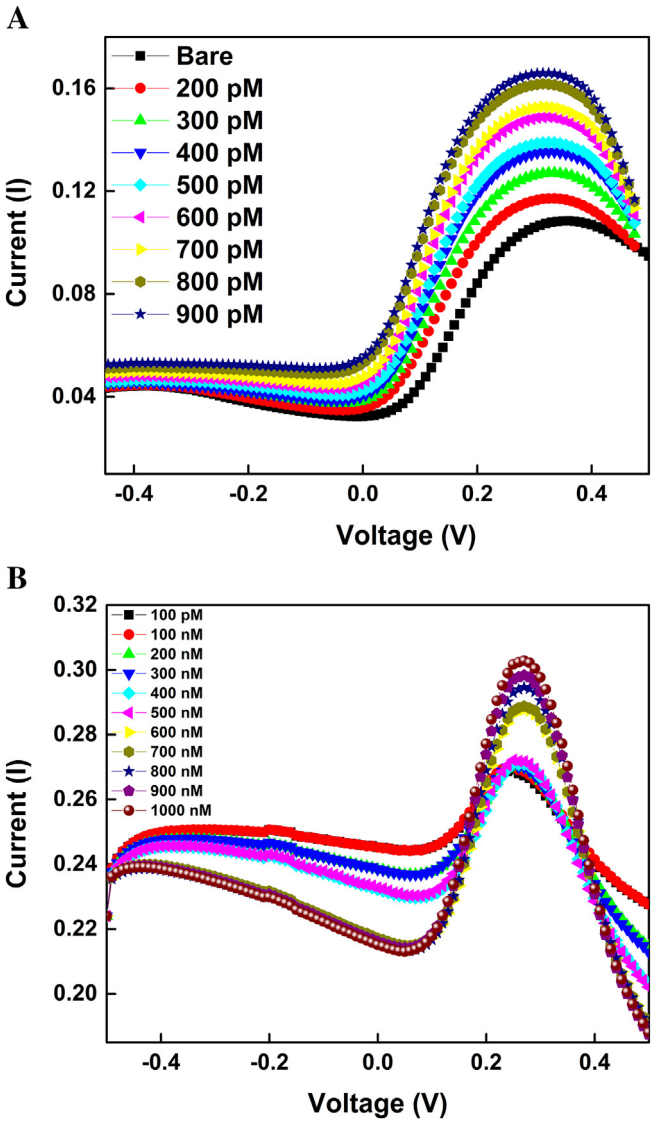

Fig. 12. A Square wave voltammetry curves of AchE-ChO/Au_{NPs}/GO electrode with Ach concentrations (lower range) varying from 200 pM to 900 pM. B Square wave voltammetry curves of AchE-ChO/Au_{NPs}/GO electrode with Ach concentrations (higher range) varying from 100 pM to 1000 nM.

as described. The above results (EIS) confirms a desirable modification occurred during the preparation of working electrode.

3.2. Voltammetric studies

Voltammetry testing were carried out on enzyme based Au_{NPs}-GO/ITO@ glass electrode in the scan range of −0.7 V to +0.8 V with 20 mV/s scan rate. The CV curves (Fig. 9A) were obtained for the Ach solutions having concentration ranging from 100 pM to 900 pM (for lower range). The oxidation and reduction peak currents indicate good electrochemical properties of the electrode. Fig. 9B illustrates the calibration curve between Ach concentrations (pM) and current response (mA). It depicts the change of sensing signal in the form of current by increasing the Ach concentrations upto 900 pM. By plotting the reciprocal of the Ach concentrations (X) and the reciprocal of the current response (Y) acquired, the affinity constant /Km for the bienzyme-based electrode was found to be 285.71 pM. The slope of the linear curve/sensitivity was calculated 0.383 mA/pM.

Fig. 10 is showing the cyclic voltammetry curves for AchE-ChO/Au_{NPs}-GO/ITO@ glass electrode in 2.5 mM ferri/ferro solution as electrolyte and 0.1 M sodium phosphate buffer (pH 7.5) by applying the potential from −0.7 to +0.8 V with varying the scan rates (10 mV/s to 100 mV/s). The rise in cathodic and anodic peak currents with the increase in scan rate indicates the homogeneous and constant electron transfer through the electrode. Fig. 11 illustrates the variation of peak current with the square root of scan rate. The linearity in the peak currents (anodic and cathodic) with scan rate signify the facile charge transfer process in the electrode which can be described by the following parameters and equations:

For anodic current:

Intercept : -0.12619 ± 0.00979

Slope : 0.08679 ± 0.00132

$Y = 0.08679\,x - 0.12619$

For cathodic current:

Intercept : 0.13056 ± 0.0137

Slope : -0.10578 ± 0.00185

$Y = -0.10578\,x + 0.13056$

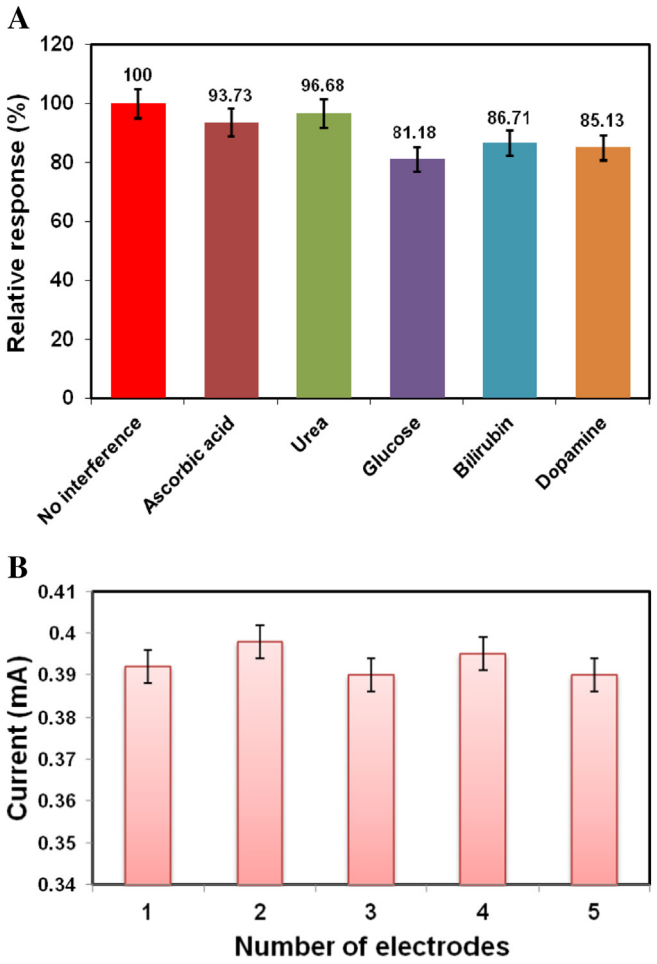

Fig. 13. A Relative response of different interfering agents is plotted with respect to Ach response. B Current response of the biosensor fabricated on five different electrodes for the detection of Ach.

Table 1
Analytical recovery of Ach in spiked serum samples using AchE-ChO/Au_{NPs}-GO/ITO@ glass electrode.

Substrate/analyte	Amount added (nM)	Amount found (nM)	Recovery (%)
Ach	1.0	0.98	98.0%

3.3. Sensing measurements

The sensing efficiency of fabricated AchE-ChO/Au_{NPs}-GO/ITO@ glass electrode was estimated using cyclic voltammetry technique in −0.7 to +0.8 V potential range and scan rate of 20 mV/s. The sensing efficiency was estimated in the concentration range of 100 pM to 1000 nM.

The data can also be correlated with that acquired with square wave pulsed voltammetry. Square wave voltammetry is employed because it gives distinctive anodic peak potentials which give a clear idea about the oxidation occurring at the surface of electrode. The substrate concentration range is divided into two categories: low range of concentrations from 200 pM to 900 pM (Fig. 12A) and high range of concentrations from 100 pM to 1000 nM (Fig. 12B). It was observed that the anodic and cathodic peak potentials exhibited a gradual rise with increasing concentration in both ranges. This technique also imparted the same gradual increase in the anodic peak potential and thus, confirms good sensing efficiency of the fabricated electrode showing the excellent charge transfer on the surface of electrode. The linearity can be inferred as the efficient sensing capability of the fabricated electrode. The detection limit for the electrode was observed to be 100 pM, which is lower than the detection limit reported earlier in literature with other electrodes modified with Fe_2O_3NPs/rGO/PEDOT [8], AchE-ChO/Pt/MOF/Au [9], AchE-ChO/Quantum dots/rGO [12], AchE-ChO/Pt/graphene [10] and Fe_3O_4 nanospheres/rGO [11]. The response time is

Table 2
Precision study for Ach determination in serum samples using AchE-ChO/Au_{NPs}-GO/ITO@glass electrode.

Substrate/analyte	Within batch ($n = 5$) Mean ± SD	Between batch (n = 5) Mean ± SD
Ach	1.04 ± 0.21	1.13 ± 0.42

Table 3
Comparison of analytical properties of present biosensor with earlier reported electrochemical interfaces.

S. no.	Type of biosensor	Matrix	Detection limit	Linear range	Response time (seconds)	References
1.	Electrochemical	Fe_2O_3NPs/rGO/PEDOT modified FTO electrode	4.0 nM	4.0 nM to 800 μM	<4	[8]
2.	Electrochemical	AchE-ChO/PtNPs/MOF cladded Au electrode	0.01 μM	0.01–500 μM	NR	[9]
3.	Electrochemiluminescence	Quantum dots/electrochemically reduced graphene oxide	4.7 μM	10–250 μM	NR	[12]
4.	Electrochemical	ITO plate modified Pt-Graphene NPs	–	0.005–700 μM	4	[10]
5.	Colorimetry	Fe_3O_4 Nano Spheres/rGO	39.0 nM	0.1–10,000 μM	NR	[11]
6.	Electrochemical	AchE-ChO-Au_{NPs}-GO/ITO@glass electrode	100 pM	100 pM to 1000 nM	3	Present

* NR = Not reported.

found to be 3 s for the measurement of current after addition of analyte i.e. Ach, which is less than the reported work on AchE-ChO/Pt/graphene modified electrode [10] and Fe_2O_3NPs/rGO/PEDOT modified FTO electrode [8].

3.4. Interference studies

Selectivity among other interfering agents is one of the important criteria for choosing a biosensor. Therefore, different common interfering agents (Ascorbic acid, Urea, Glucose, Bilirubin and Dopamine) were tested along with Ach and cyclic voltammetry curves were obtained. Anodic and cathodic currents were noted down for each interfering agent and compared with the current response for Ach as shown in Fig. 13A. Compared to Ach (1 nM), the current change caused by introduction of the five interfering compounds are <15% and so the selectivity of biosensor is acceptable.

3.5. Analysis of real samples

Five real serum samples were examined for the estimation of feasibility and applicability of the developed biosensor. Generally, 8.66 ± 1.02 nM is considered as the normal Ach level in human serum [10]. In serum samples the known concentrations of Ach solution was added and measured by the developed AchE-ChO/Au_{NPs}-GO/ITO@ glass electrode. The biosensor was evaluated to obtain important analytical parameters e.g. precision and recovery for Ach detection. The analytical recovery of the prepared biosensor is presented in Table 1. The mean analytic recovery of added Ach at final concentration of 1.0 nM (in spiked serum sample) obtained by the present biosensor was 98.0%. The other analytical property, precision of the prepared biosensor, is reported in Table 2. To test the consistency and reproducibility of the present biosensor, Ach concentration in a same serum sample was tested multiple times (5 times) in a single day (within a batch) and again after storing the same sample for one week at 4 °C (between batch). All the determined Ach concentrations were consistent. The coefficient of variation for both batches within and between was found to be 1.04% and 1.13%, respectively, which shows good reliability of the present sensing device. A comparative analysis for analytic parameters of different types of biosensors for detection of Ach with the present nanocomposite based sensor is summarized in Table 3.

3.6. Storage stability of the AchE-ChO/AuNPs-GO/ITO@ glass electrode

The stability of AchE-ChO co-immobilized Au_{NPs}-GO/ITO@ glass plate was estimated by analyzing current obtained with 1.0 nM Ach solution in a mixture of 0.1 M PBS (pH 7.5) at a regular interval of 7 days. It is observed that when as-prepared enzyme electrode was stored at 4 °C, it is capable of retaining the sensing activity upto 70% for the period of 8 weeks. It is observed that the loss in activity of enzyme electrode is mainly as a result of denaturing of the AchE-ChO (enzymes) causing an effect on the stability of AchE-ChO/Au_{NPs}-GO/ITO@ glass electrode.

The reusability of the biosensor was significantly tested through the reproducibility technique. In order to check the reusability, 0.1 mM of Ach was utilized with 5 separately fabricated electrodes. As shown in Fig. 13B, these 5 independently developed electrodes demonstrated a homogeneous current yield. A moderately lower standard deviation was obtained supporting a high repeatability and precisely reusable and reproducible quality of the present Ach biosensor.

4. Conclusions

Enzymes based Au_{NPs}-GO nanocomposite on ITO@ glass plate as working electrode was prepared. Different characterizations like UV–Visible spectroscopy, X-ray diffraction and scanning electron microscopy confirmed the presence of Au_{NPs}. Also, FTIR confirmed the attachment of AchE-ChO enzymes with the functional groups of GO. Cyclic voltammetry curves showed the sensing ability of the working electrode towards Ach concentrations ranging from 100 pM to 1000 nM. The limit of detection was found to be 100 pM. Square wave voltammetry plots also support the results and showed good anodic peak for varying concentration of Ach. Interference studies showed the good selectivity of electrode for Ach among other common interfering agents and hence this electrode can be employed as rapid and precise Ach biosensor. The present biosensor is also tested for the real sample analysis.

Declaration of competing interest

None.

Acknowledgement

Dr. Jain highly acknowledged “Start-up Research Grant” given by SERB, Department of Science & Technology (DST) (File No. YSS/2015/000023), Government of India. Chetna Tyagi is thankful to UGC for the fellowship provided.

References

[1] S.-B. He, G.-W. Wu, H.-H. Deng, A.-L. Liu, X.-H. Lin, X.-H. Xia, W. Chen, Choline and acetylcholine detection based on peroxidase-like activity and protein antifouling property of platinum nanoparticles in bovine serum albumin scaffold, Biosens. Bioelectron. 62 (2014) 331–336.
[2] P.K. Sharma, H.R. Thakur, J.C. Dutta, Modeling and simulation of carbon nanotube-based dual-gated enzyme field effect transistor for acetylcholine detection, J. Comput. Electron. 16 (3) (2017) 584–592.
[3] J.A. Zackheim, E.D. Abercrombie, HPLC/EC detection and quantification of acetylcholine in dialysates, Drugs of Abuse, Springer 2003, pp. 433–441.
[4] J. Murata, T. Watanabe, K. Sugahara, T. Yamagaki, T. Takahashi, High-resolution mass spectrometry for detecting acetylcholine in Arabidopsis, Plant Signal. Behav. 10 (10) (2015), e1074367.
[5] J. Schuberth, B. Sparf, A. Sundwall, A technique for the study of acetylcholine turnover in mouse brain in vivo, J. Neurochem. 16 (5) (1969) 695–700.
[6] J.-H. Oh, B.C. Kim, J.-S. Lee, Colorimetric detection of acetylcholine with plasmonic nanomaterials signaling, Anal. Bioanal. Chem. 406 (29) (2014) 7591–7600.
[7] J. Říčný, J. Coupek, S. Tuček, Determination of acetylcholine and choline by flow-injection with immobilized enzymes and fluorometric or luminometric detection, Anal. Biochem. 176 (2) (1989) 221–227.
[8] N. Chauhan, S. Chawla, C. Pundir, U. Jain, An electrochemical sensor for detection of neurotransmitter-acetylcholine using metal nanoparticles, 2D material and conducting polymer modified electrode, Biosens. Bioelectron. 89 (2017) 377–383.
[9] N. Chauhan, S. Tiwari, T. Narayan, U. Jain, Bienzymatic assembly formed@ Pt nano sensing framework detecting acetylcholine in aqueous phase, Appl. Surf. Sci. 474 (2018) 154–160.
[10] N. Chauhan, J. Narang, U. Jain, Highly sensitive and rapid detection of acetylcholine using an ITO plate modified with platinum-graphene nanoparticles, Analyst 140 (6) (2015) 1988–1994.

[11] J. Qian, X. Yang, L. Jiang, C. Zhu, H. Mao, K. Wang, Facile preparation of Fe3O4 nanospheres/reduced graphene oxide nanocomposites with high peroxidase-like activity for sensitive and selective colorimetric detection of acetylcholine, Sensors Actuators B Chem. 201 (2014) 160–166.
[12] S. Deng, J. Lei, L. Cheng, Y. Zhang, H. Ju, Amplified electrochemiluminescence of quantum dots by electrochemically reduced graphene oxide for nanobiosensing of acetylcholine, Biosens. Bioelectron. 26 (11) (2011) 4552–4558.
[13] Y. Shao, J. Wang, H. Wu, J. Liu, I.A. Aksay, Y. Lin, Graphene based electrochemical sensors and biosensors: a review, Electroanalysis 22 (10) (2010) 1027–1036.
[14] R.L. McCreery, Advanced carbon electrode materials for molecular electrochemistry, Chem. Rev. 108 (7) (2008) 2646–2687.
[15] S.N. Kim, J.F. Rusling, F. Papadimitrakopoulos, Carbon nanotubes for electronic and electrochemical detection of biomolecules, Adv. Mater. 19 (20) (2007) 3214–3228.
[16] Y. Shao, J. Liu, Y. Wang, Y. Lin, Novel catalyst support materials for PEM fuel cells: current status and future prospects, J. Mater. Chem. 19 (1) (2009) 46–59.
[17] K. Gong, Y. Yan, M. Zhang, L. Su, S. Xiong, L. Mao, Electrochemistry and electroanalytical applications of carbon nanotubes: a review, Anal. Sci. 21 (12) (2005) 1383–1393.
[18] G.G. Wildgoose, C.E. Banks, R.G. Compton, Metal nanoparticles and related materials supported on carbon nanotubes: methods and applications, Small 2 (2) (2006) 182–193.
[19] M. Segal, Selling graphene by the ton, Nat. Nanotechnol. 4 (10) (2009) 612.
[20] D.C. Marcano, D.V. Kosynkin, J.M. Berlin, A. Sinitskii, Z. Sun, A. Slesarev, L.B. Alemany, W. Lu, J.M. Tour, Improved Synthesis of Graphene Oxide, 2010.
[21] D. Chen, H. Feng, J. Li, Graphene oxide: preparation, functionalization, and electrochemical applications, Chem. Rev. 112 (11) (2012) 6027–6053.
[22] C. Chung, Y.-K. Kim, D. Shin, S.-R. Ryoo, B.H. Hong, D.-H. Min, Biomedical applications of graphene and graphene oxide, Acc. Chem. Res. 46 (10) (2013) 2211–2224.
[23] J. Huang, L. Zhang, B. Chen, N. Ji, F. Chen, Y. Zhang, Z. Zhang, Nanocomposites of size-controlled gold nanoparticles and graphene oxide: formation and applications in SERS and catalysis, Nanoscale 2 (12) (2010) 2733–2738.
[24] V.K. Gupta, N. Atar, M.L. Yola, M. Eryılmaz, H. Torul, U. Tamer, İ.H. Boyacı, Z. Üstündağ, A novel glucose biosensor platform based on Ag@ AuNPs modified graphene oxide nanocomposite and SERS application, J. Colloid Interface Sci. 406 (2013) 231–237.
[25] Y. Li, W. Gao, L. Ci, C. Wang, P.M. Ajayan, Catalytic performance of Pt nanoparticles on reduced graphene oxide for methanol electro-oxidation, Carbon 48 (4) (2010) 1124–1130.
[26] X. Chen, G. Wu, J. Chen, X. Chen, Z. Xie, X. Wang, Synthesis of “clean” and well-dispersive Pd nanoparticles with excellent electrocatalytic property on graphene oxide, J. Am. Chem. Soc. 133 (11) (2011) 3693–3695.
[27] X. Huang, M.A. El-Sayed, Gold nanoparticles: optical properties and implementations in cancer diagnosis and photothermal therapy, J. Adv. Res. 1 (1) (2010) 13–28.
[28] S. Abraham, N.R. Nirala, S. Pandey, M. Srivastava, S. Srivastava, B. Walkenfort, A. Srivastava, Functional graphene–gold nanoparticle hybrid system for enhanced electrochemical biosensing of free cholesterol, Anal. Methods 7 (9) (2015) 3993–4002.
[29] D. Choi, S.-J. Hong, Y. Son, Characteristics of indium tin oxide (ITO) nanoparticles recovered by lift-off method from TFT-LCD panel scraps, Materials 7 (12) (2014) 7662–7669.
[30] D. Fan, S. Wu, S. Tian, J. Zhou, Y. Ju, C. Ma, J. Shi, Detection of dopamine on a poly (metanilic acid) decorated two-dimensional gold cavity array electrode, RSC Adv. 4 (91) (2014) 49560–49568.
[31] M. Soltani Nejad, G.H. Shahidi Bonjar, N. Khaleghi, Biosynthesis of gold nanoparticles using streptomyces fulvissimus isolate, Nanomedicine Journal 2 (2) (2015) 153–159.
[32] C. Tyagi, S.A. Khan, I. Sulania, R. Meena, D.K. Avasthi, A. Tripathi, Evidence of ion-beam induced annealing in graphene oxide film using in-situ X-ray diffraction and spectroscopy techniques, J. Phys. Chem. C 122 (2018) 9632–9640.
[33] A.C. Ferrari, J. Robertson, Interpretation of Raman spectra of disordered and amorphous carbon, Phys. Rev. B 61 (20) (2000), 14095.
[34] A. Ferrari, J. Robertson, Resonant Raman spectroscopy of disordered, amorphous, and diamondlike carbon, Phys. Rev. B 64 (7) (2001), 075414.